Density Oscillations Induced by Individual Ultracold Two-Body Collisions

Q. Guan, V. Klinkhamer, R. Klemt, J. H. Becher, A. Bergschneider, P. M. Preiss, S. Jochim, and D. Blume

Phys. Rev. Lett. **122**, 083401 — Published 27 February 2019

DOI: 10.1103/PhysRevLett.122.083401

Density oscillations induced by individual ultracold two-body collisions

Q. Guan,[1] V. Klinkhamer,[2] R. Klemt,[2] J. H. Becher,[2] A. Bergschneider,[2,*] P. M. Preiss,[2] S. Jochim,[2] and D. Blume[1]

[1]*Homer L. Dodge Department of Physics and Astronomy, The University of Oklahoma, 440 West Brooks Street, Norman, Oklahoma 73019, USA*

[2]*Physics Institute, Heidelberg University, Im Neuenheimer Feld 226, 69120 Heidelberg, Germany*

(Dated: January 25, 2019)

Access to single particle momenta provides new means of studying the dynamics of few interacting particles. In a joint theoretical and experimental effort, we observe and analyze the effects of a finite number of ultracold two-body collisions on the relative and single-particle densities by quenching two ultracold atoms with initial narrow wave packet into a wide trap with inverted aspect ratio. The experimentally observed spatial oscillations of the relative density are reproduced by a parameter-free zero-range theory and interpreted in terms of cross-dimensional flux. We theoretically study the long time dynamics and find that the system does not approach its thermodynamic limit. The set-up can be viewed as an advanced particle-collider that allows one to watch the collision process itself.

PACS numbers:

The one-dimensional harmonic oscillator is discussed in many text books, from introductory classical and quantum mechanics to quantum optics and field theory [1]. The physics of the one-dimensional harmonic oscillator is simple: Its classical orbits are sinusoidal and periodic and the quantum propagator has a compact analytical expression. Moreover, the harmonic oscillator allows one to gain intuition for the dynamics of multi-dimensional systems.

This work studies, both experimentally and theoretically, the quench dynamics of an *anisotropic* three-dimensional harmonic oscillator in which the three degrees of freedom are coupled by a point scatterer of varying strength that is located at the origin. Since the point scatterer has a measure of zero, the classical trajectories are not influenced by the point scatterer [2]. However, the situation changes drastically when one enters the quantum regime since the point scatterer can simultaneously partially reflect and partially transmit the wave packet, or even reflect the wave packet in its entirety [2–15].

The quench dynamics of one-dimensional quantum systems has been investigated extensively at the microscopic level [9–12, 14–24]. Examples include the realization of quantum Newton's cradle [16, 20, 21] and the observation of quantum revivals in a system containing around 1000 atoms, addressing questions related to equilibration, thermalization, and their connections to integrability of one-dimensional systems [22]. The quench dynamics of three-dimensional systems is expected to differ from that of one-dimensional systems in important ways. This letter explores these differences by studying the quench dynamics of an anisotropic harmonic oscillator, including the weakly-attractive and repulsive regimes, where the system behavior is quite intuitive, and the strongly-interacting regime, where the s-wave scattering length is the largest length scale in the problem and intuition tends to fail.

We realize the three-dimensional anisotropic harmonic oscillator with point scatterer experimentally by optically trapping two ultracold atoms [Fig. 1(a)], which interact via a short-range van der Waals potential with tunable scattering length. The dynamics are initiated by a quench of the trap geometry. The system provides a versatile platform for studying few-body dynamics in a regime where a small and predictable number of collisions occur. Since the optical trap is nearly perfectly harmonic, the center-of-mass motion, which is not affected by the interactions, decouples from the relative motion. Thus, we focus on (i) the dynamics in the relative degrees of freedom and (ii) the impact of this motion on the single-particle density. Excellent agreement with our parameter-free theory predictions is found. In the strongly-interacting regime, the resulting density profiles in the relative, low-energy z-coordinate display time-dependent oscillatory or fringe pattern, which we interpret as signatures of cross-dimensional dynamics. The single-particle density profiles, in contrast, are smooth except for very short time periods during which the two particles are close to each other. This illustrates that the scattering events impact the single- and higher-order correlation functions differently. While the relative density varies appreciably with time, our calculations reveal an extremely slow approach to equilibrium, manifest in a failure to thermalize over thousands of cycles.

Experimentally, we prepare two ^{6}Li atoms in two distinct hyperfine states denoted by $|1\rangle$ and $|3\rangle$ [25] in the motional ground state of a tightly focussed optical tweezer trap elongated along the x-direction [Fig. 1(ai)] [26]. At time $t = 0$, the system is quenched by instantaneously changing the trap geometry and aspect ratio [Fig. 1(aii)]. We release the atoms into a much weaker dipole trap with inverted geometry, whose weakest frequency is along the z-axis. Since the trap potentials are harmonic to a good approximation, the system before and after the quench is described in terms of the low-energy two-particle Hamiltonian $H_\alpha = H_{\mathrm{rel},\alpha} +$

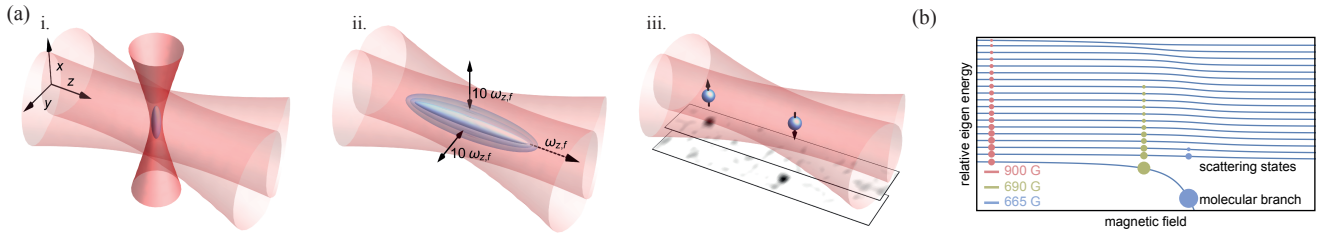

FIG. 1: (color online) Schematic of system and characterization of initial state. (ai) We prepare the wavepacket of two interacting ^{6}Li atoms (blue cloud) in the ground state of a tight optical tweezer trap (dark red). We additionaly ramp on a weak crossed beam optical dipole trap (light red, not to scale). (aii) At $t = 0$ we switch off the tweezer trap to quench the trap geometry so that the cloud quickly oscillates in the x- and y-directions while slowly expanding in the z-direction. (aiii) After a variable expansion time we record the z-positions of both atoms via fluorescence imaging. (b) Schematic energy spectrum of the Hamiltonian $H_{\mathrm{rel},f}$ after the quench, showing a single "molecular branch" and a nearly harmonic spectrum of "scattering states". Different magnetic fields lead to very different projections of the initial state onto the eigenstates of $H_{\mathrm{rel},f}$. In the weakly-interacting regime at large magnetic fields, many scattering states are populated with roughly equal probability. At lower magnetic fields, the projection onto the single molecular state increases, eventually dominating the two-body dynamics. For the experimental parameters, hundreds of levels contribute to the dynamics.

$H_{\mathrm{cm},\alpha}$, where $\alpha = i, f$ denotes the geometry before (i) and after (f) the quench,

$$H_{\mathrm{rel},\alpha} = \frac{-\hbar^2}{2\mu}\vec{\nabla}^2_{\vec{r}} + \frac{\mu}{2}(\omega^2_{x,\alpha}x^2 + \omega^2_{y,\alpha}y^2 + \omega^2_{z,\alpha}z^2) + \frac{2\pi\hbar^2 a_s}{\mu}\delta(\vec{r})\frac{\partial}{\partial r}r \quad (1)$$

and

$$H_{\mathrm{cm},\alpha} = \frac{-\hbar^2}{2M}\vec{\nabla}^2_{\vec{R}} + \frac{M}{2}(\omega^2_{x,\alpha}X^2 + \omega^2_{y,\alpha}Y^2 + \omega^2_{z,\alpha}Z^2). \quad (2)$$

Here, $\vec{r} = (x, y, z)^T$ and $\vec{R} = (X, Y, Z)^T$ are the relative and center-of-mass position vectors, respectively, μ and M the associated masses, and a_s the three-dimensional s-wave scattering length characterizing the interaction strength.

The experimentally measured trapping frequencies are $\omega_{x,i} : \omega_{y,i} : \omega_{z,i} = 2\pi \times (6.4 : 31 : 30)$ kHz before and $\omega_{x,f} : \omega_{y,f} : \omega_{z,f} = 2\pi \times (640 : 600 : 61.7)$ Hz (aspect ratio of $\omega_{x/y,f}/\omega_{z,f} \approx 10$) after the quench. For all theoretical studies presented, to simplify the calculations, we assume that the initial and final traps are axially symmetric (but about different axis). Specifically, our calculations use $\omega_{y,i} = \omega_{z,i}$, $\omega_{x,i}/\omega_{z,i} = 0.2098$, $\omega_{z,i}/\omega_{z,f} = 494.3$, $\omega_{x,f} = \omega_{y,f}$, and $\omega_{x,f}/\omega_{z,f} = 10$.

We record the spatial correlations along the z-axis [Fig. 1(aiii)] that develop during the wave packet dynamics using a single-atom and state resolved imaging scheme [27]. Furthermore, we control the interaction strength by adiabatically adjusting a magnetic offset field in the vicinity of a broad Feshbach resonance located at around 690 G [25]. This allows us to reach three distinct regimes via the quench, which are set by the role of a bound state in the system [Fig. 1(b)]: In the case of a small negative a_s [in units of the harmonic oscillator length $a_{\mathrm{ho},z} = \sqrt{\hbar/(\mu\omega_{z,f})}$], the system is in the weakly-attractive regime where the quench projects onto a large number of nearly free particle eigenstates. For $a_s/a_{\mathrm{ho},z} = -0.0203$, the occupation $|c_0|^2$ of the lowest eigenstate of $H_{\mathrm{rel},f}$ immediately after the quench is about 2% (Table S1 [28]). For small positive a_s (e.g. $a_s/a_{\mathrm{ho},z} = 0.0474$), in contrast, the particles are deeply bound into a single molecular state both before and after the quench. In this work, we are particularly interested in the paradigmatic "unitary" regime [38, 39], where the three-dimensional scattering length is the largest length scale in the system or even diverges. In this regime ($a_s/a_{\mathrm{ho},z} = -4.64$), $|c_0|^2$ is of order 0.3 (Table S1 [28]).

Since the quench does not couple the relative and center-of-mass motions, the center-of-mass wave packet for $t > 0$ simply performs breathing oscillations at the characteristic time scales $T_{x/y/z}/2 = \pi/\omega_{x/y/z,f}$. The relative motion, in contrast, is non-trivial. Since the energy $\langle E_{\mathrm{rel}}\rangle$ of the $t > 0$ wave packet in the relative degrees of freedom is much larger than the energy scales set by the trapping frequencies of $H_{\mathrm{rel},f}$ (Table S1 [28]), the dynamics in the relative degrees of freedom involves many eigenstates of $H_{\mathrm{rel},f}$. To illustrate this, the circles in Fig. 1(b) schematically show the occupation probabilities $|c_j|^2$, which are obtained by expanding the relative portion of the $t < 0$ wave packet in terms of the eigenstates of $H_{\mathrm{rel},f}$ [40, 41], for three different s-wave scattering lengths.

Figure 2 summarizes the dynamics for $a_s = -4.64a_{\mathrm{ho},z}$ by displaying $\langle\rho^2\rangle$ and $\langle z^2\rangle$, where $\rho^2 = x^2 + y^2$. Both observables oscillate smoothly with time but at different frequencies. The times marked by a circle, a square, and arrows are discussed in more detail in Figs. 3, 4, and 5, respectively.

Figure 3 shows the relative density along the z-coordinate for $t = 3.5$ ms $= 2.16T_x$, i.e., after four collisions (Fig. 2), for six different s-wave scattering lengths.

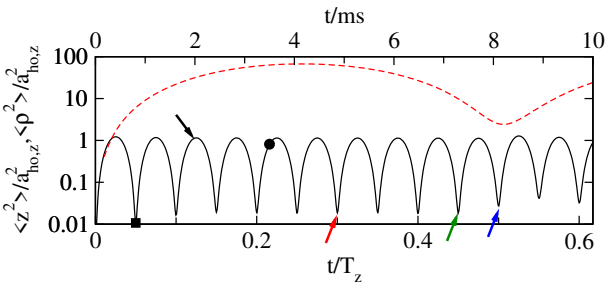

FIG. 2: (color online) Expectation values of ρ^2 (solid line) and z^2 (dashed line) for $a_s = -4.64a_{\mathrm{ho},z}$ as a function of time. The circle, square, and arrows mark the times that are considered in Figs. 3, 4, and 5, respectively.

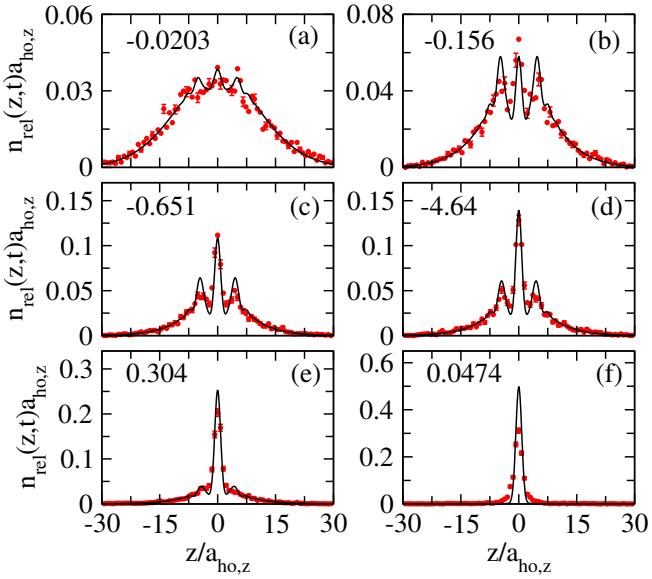

FIG. 3: (color online) Experiment-theory comparison after four two-body collisions. The relative densities $n_{\mathrm{rel}}(z,t)$ are shown for $t = 3.5$ ms and six different scattering lengths. The values of a_s (in units of $a_{\mathrm{ho},z}$) are reported in the upper left corner of each panel. Circles show experimental data and solid lines convolved theory results. Typical error bars are shown for a subset of the experimental data. Note the different y-scales in the panels.

The agreement between the experimental results (circles) and the parameter-free theory results (solid lines) is, except for Fig. 3(f), very good. The theoretical results shown in Fig. 3 are convolved with a Gaussian to account for the experimental resolution of 4 $\mu m = 0.542a_{\mathrm{ho},z}$. Interestingly, the relative densities shown in Figs. 3(a)-3(e) contain oscillatory structure or fringes, which change notably with the s-wave scattering length a_s, on top of a broad background. The fringe pattern changes with time and we have found no unique way to assign t- and z-independent peak spacings for fixed scattering length. For the smallest positive s-wave scattering length considered [Fig. 3(f)], the initial state is small compared to the harmonic oscillator lengths of the final and initial traps and the coefficient $|c_0|^2$ is large (Table S1 [28]). In this case, finite-range effects might need to be accounted for to obtain quantitative agreement between theory and experiment.

The relative densities, shown in Figs. 3(a)-3(f), reflect the evolution from a comparatively weakly-interacting regime, in which the molecular state does not play a special role (small $|c_0|^2$), to the strongly-interacting regime, where $|c_0|^2$ is appreciable but not dominant, to the small molecular bound-state regime, where $|c_0|^2$ dominates. For large negative a_s we observe a clear fringe pattern. Since the wave packet in the relative coordinate would, in the absence of the scatterer, simply repeatedly expand and contract, the fringes have to be caused by scattering events. Figure 4 shows the theoretically determined unconvolved relative density along z for $a_s = -0.651a_{\mathrm{ho},z}$ during the first scattering event, i.e., for t close to $t = T_x/2$. At this time, $\langle\rho^2\rangle$ is quite small but $\langle z^2\rangle$ is comparatively large. This implies that the majority of the wave packet is located away from the point scatterer. The snapshots in Fig. 4 illustrate that the fringes emerge as a consequence of the scattering. A portion of the small-ρ wave packet does not get reflected along the ρ-direction but instead gets "redirected" to leave the small-ρ region along the z-direction [schematic in Fig. 4(g)]. One can think of the scattering event as a cross-dimensional redistribution of flux from the ρ- to the z-direction, creating a newly emitted wave packet portion along the z-direction that subsequently interferes with the "background" wave packet portion. This process is repeated during subsequent scattering events ($t \approx nT_x/2; n = 2, 3, 4, ...$), leading to an increasingly complex fringe pattern in the relative density along z (see also Fig. S3 [28]).

Does the single-particle density, an observable recorded frequently in cold atom experiments, develop a fringe pattern? The answer is yes but only for very short time periods over a length scale that is too small to be observed with the current experimental set-up. Figure 5(a) compares the experimental (diamonds) and convolved theoretical (solid line) single-particle densities along z for $t = 2$ms and $a_s = -4.64a_{\mathrm{ho},z}$. At this time, which corresponds to two oscillations of $\langle\rho^2\rangle$ (Fig. 2), the convolved single-particle density is smooth. It continues to be smooth for times $t < 0.5T_z$ [red dashed and green dot-dashed lines in Fig. 5(a)]. Since the size of the wave packet is much larger than the Gaussian convolution width σ, $\sigma = 0.542a_{\mathrm{ho},z}$, the convolved and unconvolved single-particle density are indistinguishable on the scale shown in Fig. 5(a). The behavior of the single-particle density changes drastically when the wave packet is characterized by a small $\langle z^2\rangle$ and a small $\langle\rho^2\rangle$. For $t \approx 0.5T_z$, the unconvolved single-particle density [solid

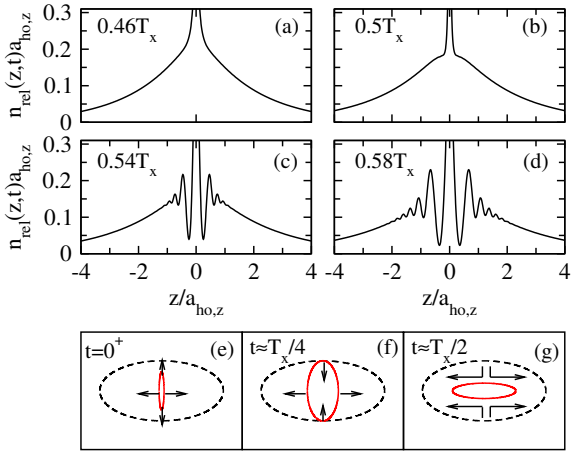

FIG. 4: (color online) Development of fringe pattern in the relative density during the first collision event ($t \approx T_x/2$) for $a_s = -0.651 a_{\mathrm{ho},z}$. (a)-(d) The lines show the theoretically determined unconvolved relative density $n_{\mathrm{rel}}(z,t)$ for the times t reported in the upper left corner of each panel. (e)-(g) The red solid lines schematically show the wave packet at (e) $t = 0^+$, (f) $t \approx T_x/4$, and (g) $t \approx T_x/2$. The black dashed lines schematically show the equipotential lines of the final trap. The arrows schematically indicate the flux.

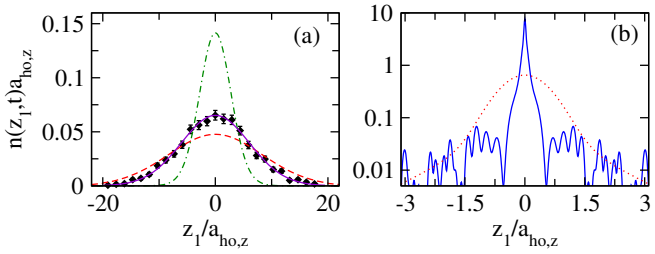

FIG. 5: (color online) Single-particle densities for $a_s = -4.64 a_{\mathrm{ho},z}$. (a) The black solid line and purple diamonds with error bars show the convolved theoretical data and experimental results for $t = 1.234 T_x = 2$ms; the red dashed and green dot-dashed lines show the convolved theoretical data for $t = 3T_x$ and $t = 4.5T_x$, respectively. (b) The blue solid and red dotted lines show, respectively, the unconvolved and convolved theoretical data for $t = 5T_x = 0.5T_z$.

line in Fig. 5(b)] exhibits a fringe pattern. The fringe pattern exists only for a short time period. For $t = 0.501T_z$ (not shown), e.g., the oscillations are no longer visible. Additionally, the limited spatial resolution smoothes out the fringe pattern of the single-particle density such that it cannot be observed in the experiment [dotted line in Fig. 5(b)]. The fringe pattern in the single-particle density keeps "appearing" and "disappearing" at larger times. Figure 6(b) shows that the single-particle density displays intricate fine structure for $t = 4T_z$ (corresponding to $\langle z^2 \rangle \approx 0$). Figure 6(d) shows that no fringe pattern exists in the single-particle density for $t = 4.25T_z$ (corresponding to $\langle z^2 \rangle \approx 70 a_{\mathrm{ho,z}}^2$). Remarkably, the relative density along z is characterized by notable fine structure for both times [Figs. 6(a) and 6(c)].

The discussion surrounding Figs. 3-6(d) illustrates that collisions impact the single-particle and relative densities differently. In particular, the relative density displays an increasingly large number of oscillations with increasing time while the single-particle density is smooth for all times, except for $t \approx nT_z/2$. Given the strong time dependence of the relative density, we ask whether the system, in the large time limit, approaches thermal equilibrium. The answer is, as is expected from Ref. [5], that it does not. To gain insight into the long-time dynamics, we analyze cycle-averaged observables, i.e., observables averaged over a period of length T_z [from $t = nT_z$ to $t = (n+1)T_z$]. Lines in Figs. 6(e) and 6(f) show the unconvolved cycle-averaged relative and single-particle densities $\langle n_{\mathrm{rel}}(z,t) \rangle_{T_z}$ and $\langle n(z_1,t) \rangle_{T_z}$, respectively, for $a_s = -4.64 a_{\mathrm{ho},z}$ and $n = 1$, 10^2, and 10^4. In both panels, the three curves are indistinguishable on the scale shown. Thus, despite the intricate dynamics within each cycle, the cycle-averaged observables display essentially no dynamics. The reason for this is that the normalized nearest neighbor energy spacings are rather sharply peaked around 1 (Fig. S1 [28]). We emphasize that this behavior is also observed for other scattering lengths. The close to frozen cycle-averaged relative density for large n indicates a lack of thermalization. Indeed, the thermal relative density [green solid line in Fig. 6(e)] differs visibly from the calculated cycle-averaged relative densities.

In summary, we have presented a joint theoretical-experimental study that investigated the wave packet dynamics of two ultracold atoms following a "violent" trap quench, which leads to the occupation of many eigenstates of the post-quench Hamiltonian. Following the quench, two-body collisions, through their effect on the structural observables, were observed. The excellent agreement between the experimental and theoretical data together with the time-resolved single-atom detection with high spatial resolution makes the system a promising candidate for future dynamical studies, which are aimed at addressing questions related to thermalization, state engineering, chaos, and integrability. The set-up also promises to be a fertile playground for testing hydro-dynamical formulations [42–44], which can potentially be used to simulate the dynamics of few- and many-body systems. Quantitative tests of the hydrodynamics theory with ultracold atoms may yield insights into why the dynamics of quark gluon plasmas seems, somewhat surprisingly, to be governed by hydrodynamic equations [45, 46].

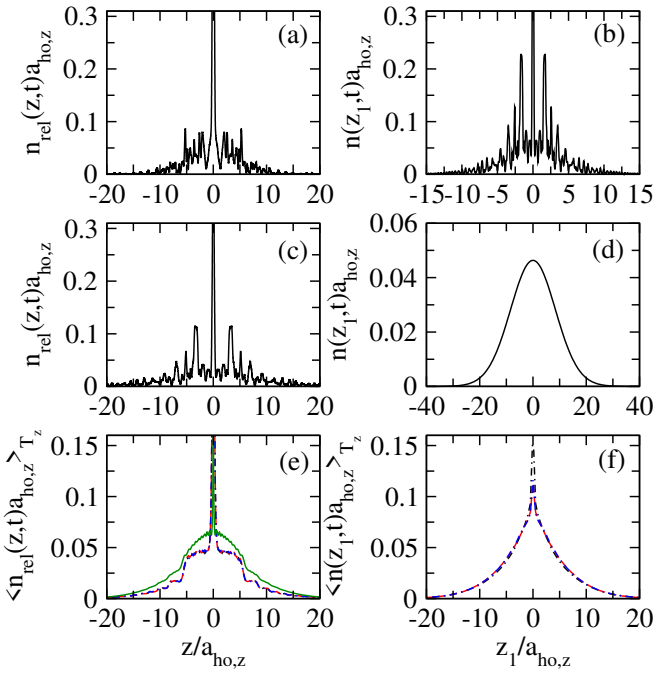

FIG. 6: (color online) Unconvolved theory results for the long-time regime for $a_s = -4.64a_{\mathrm{ho},z}$. The left and right columns show the relative and single-particle densities, respectively. Panels (a) and (b) show snapshots for $t = 4T_z$ while panels (c) and (d) show snapshots for $t = 4.25T_z$. Lines in panels (e) and (f) show cycle-averaged observables for $n = 1$, 10^2, and 10^4. On the scale shown, the lines are essentially indistinguishable. For comparison, the green solid line in panel (e) shows the relative thermal density.

ACKNOWLEDGEMENT

QG and DB gratefully acknowledge support by the National Science Foundation through grant number PHY-1806259. This work has partially been supported by the ERC consolidator grant 725636, the Heidelberg Center for Quantum Dynamics, and the DFG Collaborative Research Centre SFB 1225 (ISOQUANT). PMP acknowledges funding from European Unions Horizon 2020 programme under the Marie Sklodowska-Curie grant agreement No. 706487 and the Daimler and Benz Foundation. AB acknowledges funding from the International Max-Planck Research School (IMPRS-QD). This work used the OU Supercomputing Center for Education and Research (OSCER) at the University of Oklahoma (OU).

* Current address: Institute of Quantum Electronics, ETH Zurich, CH-8093 Zurich, Switzerland

[1] H. Kleinert, *Path Integrals in Quantum Mechanics, Statistics, Polymer Physics, and Financial Markets*, 5th ed, (World Scientific, 2009).
[2] P. Šeba, Wave Chaos in Singular Quantum Billiard, Phys. Rev. Lett. **64**, 1855 (1990).
[3] P. Šeba and K. Życzkowski, Wave Chaos in quantized classically nonchaotic systems, Phys. Rev. A **44**, 3457 (1991).
[4] S. Albeverio and P. Šeba, Wave Chaos in Quantum Systems with Point Interaction, J. Stat. Phys. **64**, 369 (1991).
[5] V. A. Yurovsky and M. Olshanii, Restricted thermalization for two interacting atoms in a multimode harmonic waveguide, Phys. Rev. A **81**, 043641 (2010).
[6] V. A. Yurovsky and M. Olshanii, Memory of the Initial Conditions in an Incompletely Chaotic Quantum System: Universal Predictions with Application to Cold Atoms, Phys. Rev. Lett. **106**, 025303 (2011).
[7] V. A. Yurovsky, A. Ben-Reuven, and M. Olshanii, Dynamics of Relaxation and Fluctuations of the Equilibrium State in an Incompletely Chaotic System, J. Phys. Chem. B **115**, 5340 (2011).
[8] A. G. Sykes, J. P. Corson, J. P. D'Incao, A. P. Koller, C. H. Greene, A. M. Rey, K. R. A. Hazzard, and J. L. Bohn, Quenching to unitarity: Quantum dynamics in a three-dimensional Bose gas, Phys. Rev. A **89**, 021601(R) (2014).
[9] J. P. Corson and J. L. Bohn, Bound-state signatures in quenched Bose-Einstein condensates, Phys. Rev. A **91**, 013616 (2015).
[10] M. Ebert, A. Volosniev, and H.-W. Hammer, Two cold atoms in a time-dependent harmonic trap in one dimension, Annalen der Physik **528**, 693 (2016).
[11] S. E. Gharashi and D. Blume, Broken scale invariance in time-dependent trapping potentials, Phys. Rev. A **94**, 063639 (2016).
[12] J. P. Corson and J. L. Bohn, Ballistic quench-induced correlation waves in ultracold gases, Phys. Rev. A **94**, 023604 (2016).
[13] C. Qu, L. P. Pitaevskii, and S. Stringari, Expansion of harmonically trapped interacting particles and time dependence of the contact, Phys. Rev. A **94**, 063635 (2016).
[14] M. A. García-March, T. Fogarty, S. Campbell, T. Busch, and M. Paternostro, Non-equilibrium thermodynamics of harmonically trapped bosons, New J. Phys. **18**, 103035 (2016).
[15] L. M. A. Kehrberger, V. J. Bolsinger, and P. Schmelcher, Quantum dynamics of two trapped bosons following infinite interaction quenches, Phys. Rev. A **97**, 013606 (2018).
[16] T. Kinoshita, T. Wenger, and D. S. Weiss, A quantum Newton's cradle, Nature **440**, 900 (2006).
[17] S. Hofferberth, I. Lesanovsky, B. Fischer, T. Schumm, and J. Schmiedmayer, Non-equilibrium coherence dynamics in one-dimensional Bose gases, Nature **449**, 324 (2007).
[18] M. Gring, M. Kuhnert, T. Langen, T. Kitagawa, B. Rauer, M. Schreitl, I. Mazets, D. Adu Smith, E. Demler, and J. Schmiedmayer, Relaxation and Prethermalization in an Isolated Quantum System, Science **337**, 1318 (2012).
[19] S. Trotzky, Y.-A. Chen, A. Flesch, I. P. McCulloch, U. Schollwöck, J. Eisert, and I. Bloch, Probing the relaxation towards equilibrium in an isolated strongly correlated 1D Bose gas, Nature Physics **8**, 325 (2012).

[20] Y. Tang, W. Kao, K.-Y. Li, S. Seo, K. Mallayya, M. Rigol, S. Gopalakrishnan, and B. L. Lev, Thermalization near integrability in a Dipolar Quantum Newton's Cradle, Phys. Rev. X **8**, 021030 (2018).

[21] C. Li, T. Zhou, I. Mazets, H.-P. Stimming, Z. Zhu, Y. Zhai, W. Xiong, X. Zhou, X. Chen, and J. Schmiedmayer, Dephasing and Relaxation of Bosons in 1D: Newton's Cradle Revisited, arXiv:1804.01969 (2018).

[22] S. Erne, R. Bücker, T. Gasenzer, J. Berges, and J. Schmiedmayer, Universal dynamics in an isolated one-dimensional Bose gas far from equilibrium, Nature **563**, 225 (2018).

[23] M. Rigol, V. Dunjko, V. Yurovsky, and M. Olshani, Relaxation in a Completely Integrable Many-Body Quantum System: An *Ab Initio* Study of the Dynamics of the Highly Excited States of 1D Lattice Hard-Core Bosons, Phys. Rev. Lett. **98**, 050405 (2007).

[24] M. Rigol, Breakdown of Thermalization in Finite One-Dimensional Systems, Phys. Rev. Lett. **103**, 100403 (2009).

[25] G. Zürn, T. Lompe, A. N. Wenz, S. Jochim, P. S. Julienne, and J. M. Hutson, Precise Characterization of ^{6}Li Feshbach Resonances Using Trap-Sideband-Resolved RF Spectroscopy of Weakly Bound Molecules, Phys. Rev. Lett. **110**, 135301 (2013).

[26] F. Serwane, G. Zürn, T. Lompe, T. B. Ottenstein, A. N. Wenz, S. Jochim, Deterministic Preparation of a Tunable Few-Fermion System, Science **332**, 6027 (2011).

[27] A. Bergschneider, V. M. Klinkhamer, J. H. Becher, R. Klemt, G. Zürn, P. M. Preiss, and S. Jochim, Spin-resolved single-atom imaging of ^{6}Li in free space, Phys. Rev. A **97**, 063613 (2018).

[28] See the supplemental material for experimental and theoretical details, which includes Refs. [29–37].

[29] T. Busch, B.-G. Englert, K. Rzążewski, and M. Wilkens, Two Cold Atoms in a Harmonic Trap, Found. Phys. **28**, 549 (1998).

[30] O. Bohigas, M. J. Giannoni, and C. Schmit, Characterization of Chaotic Quantum Spectra and Universality of Level Fluctuation Laws, Phys. Rev. Lett. **52**, 1 (1984).

[31] O. Bohigas, M. J. Giannoni, and C. Schmit, Spectral properties of the Laplacian and random matrix theories, J. Physique Lett. **45**, 1015 (1984).

[32] T. H. Ezer and R. Kosloff, An accurate and efficient scheme for propagating the time dependent Schrödinger equation, J. Chem. Phys. **81**, 3967 (1984).

[33] C. R. Monroe, E. A. Cornell, C. A. Sackett, C. J. Myatt, and C. E. Wieman, Measurement of Cs-Cs elastic scattering at $T = 30\ \mu K$, Phys. Rev. Lett. **70**, 414 (1993).

[34] H. Wu and C. J. Foot, Direct simulation of evaporative cooling, J. Phys. B **29**, 321 (1996).

[35] G. M. Kavoulakis, C. J. Pethick, and H. Smith, Relaxation Processes in Clouds of Trapped Bosons above the Bose-Einstein Condensation Temperature, Phys. Rev. Lett. **81**, 4036 (1998).

[36] B. DeMarco, J. L. Bohn, J. P. Burke, Jr., M. Holland, and D. S. Jin, Measurement of p-Wave Threshold Law Using Evaporatively Cooled Fermionic Atoms, Phys. Rev. Lett. **82**, 4208 (1999).

[37] J. Goldwin, S. Inouye, M. L. Olsen, and D. S. Jin, Cross-dimensional relaxation in Bose-Fermi mixtures, Phys. Rev. A **71**, 043408 (2005).

[38] S. Giorgini, L. P. Pitaevskii, and S. Stringari, Theory of ultracold atomic Fermi gases, Rev. Mod. Phys. **80**, 1215 (2008).

[39] I. Bloch, J. Dalibard, and W. Zwerger, Many-body physics with ultracold gases, Rev. Mod. Phys. **80**, 885 (2008).

[40] Z. Idziaszek and T. Calarco, Two atoms in an anisotropic harmonic trap, Phys. Rev. A **71**, 050701(R) (2005).

[41] Z. Idziaszek and T. Calarco, Analytical solutions for the dynamics of two trapped interacting ultracold atoms, Phys. Rev. A **74**, 022712 (2006).

[42] J.-S. Caux, B. Doyon, J. Dubail, R. Konik, and Takato Yoshimura, Hydrodynamics of the interacting Bose gas in the Quantum Newton Cradle setup, arXiv:1711.00873 (2017).

[43] X. Cao, V. B. Bulchandani, and J. E. Moore, Incomplete Thermalization from Trap-Induced Integrability Breaking: Lessons from Classical Hard Rods, Phys. Rev. Lett. **120**, 164101 (2018).

[44] M. Schemmer, I. Bouchoule, B. Doyon, and J. Dubail, Generalized HydroDynamics on an Atom Chip, arXiv:1810.07170 (2018).

[45] D. A. Teaney, *Quark Gluon Plasma 4*, (World Scientific, Singapore, 2009), p. 207.

[46] The STAR Collaboration, Global Λ hyperon polarization in nuclear collisions, Nature **548**, 62 (2017).